Oxide Film Formation at a Microcrystalline Al Alloy in Room Temperature Neutral Borate Solution

S. C. Thomas* and V. I. Birss*

Department of Chemistry, The University of Calgary, Calgary, Alberta, Canada T2N 1N4

ABSTRACT

The differences in the electrochemical behavior of a rapidly solidified, two-phase (matrix and dispersoid) microcrystalline Al-based alloy containing Fe, V, and Si (FVS0812 alloy), the bulk forms of its phases, and polycrystalline Al were investigated in neutral borate buffer solution. FVS0812 shows higher activity than the matrix and pure Al, while the dispersoid is the most active, due to oxygen evolution and dissolution, even in this benign solution. Barrier oxide films formed at FVS0812 appear to be generally uniform and similar in thickness to those formed at the matrix material. At low anodizing voltage the dispersoid phase appears to form an oxide film, although some loss of Fe and V is inferred. However, at higher voltages, evidence for the incomplete oxidation of the dispersoid phase and its incorporation and/or subsequent loss from some sites in the oxide film is seen, leading to a more flawed film of less uniform thickness. The higher capacitance of the oxide film at FVS0812 compared to that of films formed under identical conditions at Al and the matrix is consistent with the penetration of solution, via flaws, into the oxide film and the development of regions of thinner oxide film at dispersoid containing sites.

Introduction

In recent years, the technique of rapid solidification of molten metal has led to the development of new alloys which are intermediate in nature between crystalline and amorphous materials. These microcrystalline alloys possess improved properties that are unobtainable by conventional casting methods.[1,2] The microcrystalline, Al-based alloy under research, designated as FVS0812 by its developer, Allied Signal Inc., is a rapidly solidified alloy containing the elements Fe, V, and Si in addition to Al. Table I summarizes the atomic and weight percents of the elemental components of FVS0812.[3] A description of the two-phase microstructure is detailed in previous papers.[4-8] Briefly, the microstructure of alloy FVS0812 consists of nanometer-sized (*ca.* 50 nm), nearly spherical, intermetallic "dispersoids," of nominal composition $Al_{13}(Fe,V)_3Si$, uniformly distributed throughout an Al-rich matrix phase of microcrystalline grain size.

In spite of the many advantages inherent in rapidly solidified Al-based alloys,[7,9,10] an undesirable property of alloy FVS0812 is its reported inability to form a thick, porous, protective oxide film using either regular or hard anodizing methods.[8,11] In contrast to the porous oxide film produced on conventional Al alloys, which can be 60 to 100 μm in thickness, the oxide film on alloy FVS0812 reaches a limiting thickness of *ca.* 2 μm. Moreover, the oxide film which does form at FVS0812 can be removed relatively easily.

The overall goal of this research project was to establish the reasons for the FVS0812 alloy's inability to form a strong, adherent, thick, porous oxide film. As it was considered that a contribution to the difficulties inherent in the anodization of alloy FVS0812 in acidic medium, compared to pure Al and cast alloys, might arise from the properties of the barrier oxide film underlying the porous oxide,[8] the work reported in this paper focuses on oxidation of FVS0812 in barrier-film-forming, neutral boric acid/sodium borate solution. The primary objective of the present work was to evaluate barrier film formation at FVS0812 by carrying out comparative studies of the behavior of pure Al, the bulk forms of the matrix phase, and the intermetallic dispersoid phase of the alloy, and the FVS0812 alloy itself in pH 7 solution. It is shown that even in the neutral borate medium, FVS0812 does not passivate as well as does Al, probably due to more active electrochemistry of the dispersoid phase. Transmission electron microscopy (TEM) and impedance results suggest that the dispersoids introduce regions which are thinner and/or flawed in the oxide film formed at FVS0812.

* Electrochemical Society Active Member.

Table I. Composition of alloy FVS0812.

Element	Atomic percent (a/o)	Weight percent (w/o)
Al	93.2	88.5
Fe	4.3	8.5
V	0.8	1.3
Si	1.7	1.7

Experimental

Electrodes and cells.—The working electrodes (WE) employed in this study and the electrode surface preparation methods have been described previously.[8] Briefly, the WEs included a pure polycrystalline Al rod (geometric area of exposed surface *ca.* 0.32 cm^2), the extruded form of alloy FVS0812 (rod, *ca.* 0.27 cm^2), single-phase material considered to be equivalent in composition to the matrix phase of the alloy and referred to as "matrix" (rod, *ca.* 0.20 cm^2), and single-phase material considered to be equivalent in composition to the intermetallic phase of the alloy[12] and referred to as "dispersoid" (chip, *ca.* 0.25 cm^2). Electrodes were covered by an inert resin except for the exposed cross-sectional working surface area. Surface preparation, which preceded every trial, consisted of hand polishing the dispersoid electrode, while fresh surfaces of the other WEs were obtained by machine lathing at 1000 rpm for pure Al and the matrix material and 2000 rpm for alloy FVS0812. This was followed by a cleaning and rinsing process.[8] All current densities (*i*), impedances (*Z*), resistances (*R*), and capacitances (*C*) are reported with respect to the WE geometric surface area in this paper.

The three-compartment glass cell arrangement has been detailed previously.[8] The reference electrodes (RE) were either a calibrated iridium oxide electrode [*ca.* 0.43 V *vs.* the standard hydrogen electrode (SHE)] or a saturated calomel electrode. All potentials are referenced to the SHE in this paper. For work involving electrochemical impedance spectroscopy (EIS), a fourth electrode, a smooth Pt wire, was placed in the WE compartment and connected to the RE via a 6.8 μF capacitor to reduce phase shift errors at high frequencies, due to the high ohmic RE system. For work at constant potential, a Pt counterelectrode was positioned directly in the WE compartment and no RE was used.

Electrochemical instrumentation.—The electrochemical instrumentation employed has been described previously.[8] Experiments were carried out utilizing either an EG&G PAR 273 potentiostat/galvanostat or an EG&G PAR 173 combined with a PARC 175 function generator. The electrochemical data were plotted on a Hewlett Packard

7045B X/Y recorder. A Kepco power supply was used for work at constant voltage while the current/time transients were plotted on a Linear strip chart recorder. A Solartron Schlumberger 1255 HF frequency response analyzer connected to a Solartron Schlumberger 1286 electrochemical interface was used for impedance measurements, carried out at 0.1 V *vs.* SHE in neutral solution, using a constant perturbating signal amplitude of *ca.* 5 mV_{rms} over a typical frequency range of 10^0 to 10^5 Hz. The data were collected using Z-PLOT software by Scribner Associates and analyzed with EQUIVALENT CIRCUIT Version 4.51 software by Boukamp, University of Twente. Best-fit equivalent circuits, modeling the various oxide-coated substrates under study, were selected on the basis of the lowest value of the χ^2 error, and on reasonable, low errors of the fitted values of the circuit elements.

Solutions and solution analysis.—The neutral solution used was 0.5 mol $liter^{-1}$ boric acid/0.025 mol $liter^{-1}$ sodium borate, a buffer solution of pH 7.0, prepared with A. C. S. reagent grade chemicals and triply distilled water. Solutions were usually stirred and deaerated by bubbling argon gas through the solution before and during the experiment, although occasionally this was not done for work at constant potential. The temperature of the solution in the cell was usually controlled at 20 ± 5°C, although occasionally it was allowed to reach ambient temperature.

Solutions used in the electrochemical experiments were analyzed to establish the extent of metal dissolution by using either a ARL 35 000 C, ARL 3510, or Thermo Jarrell Ash Atom Scan 16 inductively coupled plasma-atomic emission spectrometer (ICP-AES).

Surface analysis.—Thin sections (*ca.* 30 nm) of selected surfaces were prepared by ultramicrotomy using either an RMC MT 6000 or a Reichert/Jung Ultracut E ultramicrotome and examined with either a Hitachi H 7000, Hitachi H 9000, or Philips 400 transmission electron microscope (TEM), as described previously.[8] The composition of the ultramicrotomed sections was determined by energy dispersive x-ray analysis (EDX) using an Oxford Instruments Link AN 10 000 attached to the Hitachi H 7000 and H 9000 TEM.

Results and Discussion

Oxide growth at constant voltage.—A series of experiments was performed in which the currents at the four WEs under study were monitored at various constant potentials after stepping or scanning at 100 mV/s from the open-circuit potential. As shown in Fig. 1, for all substrates, the current at constant voltage decreased with time, displaying an *i/t* transient typical of Al in neutral solution.[13,14] In this work, at a potential of 10 V, the steady-state leakage current at pure Al after 30 min was *ca.* 0.003 mA/cm^2 (Fig. 1), comparable to that reported by others for Al.[15] There was a significant difference in the magnitudes of the final leakage currents of the substrates under study, with that of pure Al and the matrix material being similar and less than that of the alloy, which, in turn, was substantially less than that of the dispersoid (Fig. 1). At 10 V, after 0.5 h, the current densities observed at pure Al, the matrix material, alloy FVS0812, and the bulk dispersoid were 2.8×10^{-3}, 5.1×10^{-3}, 3.6×10^{-2}, and 3.0×10^{-1} mA/cm^2, respectively. Normalized to the current density of pure Al, this provides a sequence of electrochemical activity, at 10 V, of 1 to 1.8 to 13 to 110 for pure Al, the matrix, FVS0812, and the dispersoid. During oxidation at 50 V, the disparities in the current densities became even greater, providing relative ratios, at 0.5 h, of 1 to 6 to 40 to 220 for pure Al, the matrix, FVS0812, and the dispersoid material, respectively.

For pure Al and the matrix, which are not expected to dissolve significantly in room temperature neutral solutions,[13,16,17] this steady-state current observed after 0.5 h may be considered to be a combination of electronic current through conducting pathways in the film caused by flaws arising from impurities and/or locally thinner regions of oxide, allowing oxygen evolution to occur at the oxide surface,[17] as well as continuing slow oxide growth due to the passage of ionic current.[18] The evolution of oxygen observed visually at the surface of the dispersoid material in neutral solution is consistent with the relatively high leakage current measured for that substrate. Clearly, the anodic oxide film formed at the dispersoid phase does not provide equivalent protection to the underlying substrate as it does for pure Al and the matrix material. However, the oxidation of water at the dispersoid surface contributes only partially to the anodic charge passed during polarization at positive potentials. In fact, the dissolution of the bulk dispersoid, a phenomenon that would contribute to the high anodic leakage currents, has been confirmed by ICP-AES solution analysis. Whereas no ions were detected in solution after anodization of pure Al, the matrix or FVS0812 for 0.5 h at either 10 or 50 V, the solutions in which the dispersoid was oxidized under the same conditions contained measurable levels of Al and Fe.

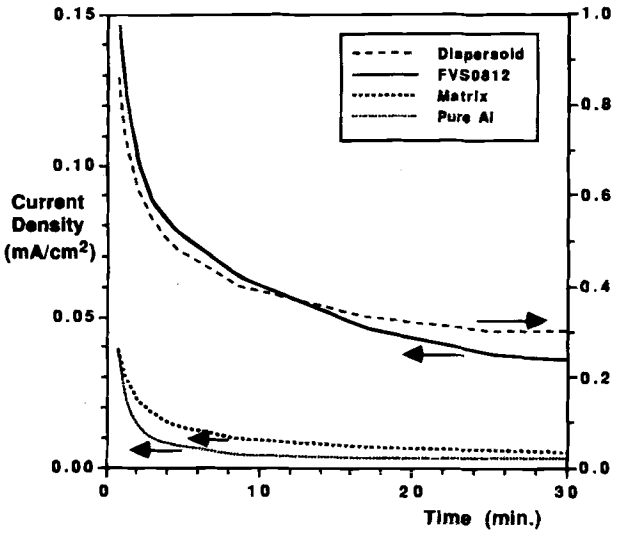

Fig. 1. Current densities observed at pure Al, the matrix, alloy FVS0812, and the dispersoid at 10 V in 20°C neutral boric acid/sodium borate.

At all potentials, the *i/t* transients and the magnitudes of the currents at FVS0812 suggest that a predominately barrier film is formed at the alloy surface in neutral borate solution. The excess leakage current at the FVS0812 alloy, compared to pure Al and the matrix material, is undoubtedly related to the presence of the dispersoid phase. Although visually unnoticeable at 10 V, evolution of oxygen at the alloy surface was observed at 50 V, suggesting that the oxide film at the alloy's surface is more flawed than is the barrier oxide film formed under comparable conditions at pure Al and the matrix. Although dissolution of the dispersoid phase can clearly occur under these conditions, no dissolved Fe or V could be detected by ICP solution analysis following anodization of the alloy at 10 and 50 V. This may indicate that the presence of the adjacent matrix phase partially protects the dispersoid in the alloy from high rates of dissolution. The significantly larger leakage currents for FVS0812, *vs.* pure Al and the matrix material, shown in Fig. 1, may therefore be attributed to continuing oxide growth at the matrix phase, perhaps very low rates of dispersoid dissolution and primarily oxygen evolution at the poorly protected dispersoid sites.

In summary, the work at constant voltage provides a sequence of electrochemical activity. The dispersoid material, displaying the highest leakage currents due to both oxygen evolution and some metal dissolution, has a significantly greater activity than that of alloy FVS0812, the activity of which, in turn, is greater than the similar activity of pure Al and the matrix material.

Potentiodynamic studies.—After an extensive literature search on the electrochemical behavior of Al and its alloys

in barrier-film-forming solution, it was established that little work based on potentiodynamic methods has been reported previously.[19-29] In the present work, cyclic voltammetry (CV) was used to examine differences in the electrochemical behavior of the substrates during the early stages of barrier film formation. Figure 2 compares the CVs of pure Al, the bulk matrix material, alloy FVS0812, and the bulk dispersoid material at a sweep rate of 100 mV/s in neutral boric acid/sodium borate. For all substrates, an anodic peak is seen at the negative end in the first anodic potential scan. Barrier film formation for pure Al and the matrix is evidenced by quasi-stationary plateau current during the anodic sweep, consistent with the literature.[23] Importantly, the CV responses of the pure Al and the matrix material are seen to be virtually indistinguishable from each other.

Figure 2 shows that all substrates exhibit significantly lower current on the first cathodic sweep. There is almost no anodic current on the second and subsequent anodic sweeps until potentials approaching the previous upper limit are reached (shown in Fig. 2 inset for the matrix substrate). This is indicative of barrier oxide formation at all four substrates. The CVs for pure Al, the matrix, and FVS0812 exhibit a type of hysteresis behavior upon reversal of sweep direction at the upper potential limit on the second and subsequent cycles (not shown), in which the current on the cathodic sweep is greater than that on the anodic sweep. This phenomenon may be related to what has been variously described as the relaxation of faradic processes at the barrier oxide/solution interphase[30] or the decay of the mobile ionic space charge layer in passive films.[31,32] As this hysteresis behavior is not observed with the dispersoid material, the formation of a different type of oxide film at the dispersoid is suggested.

Consistent with the results at constant voltage (Fig. 1), the dispersoid displays the highest activity of all the substrates (Fig. 2), with a plateau current seen up to *ca.* 1.5 V, followed by a linearly increasing current with a further increase in potential. As the intermetallic dispersoid is composed of *ca.* 76 atom percent (a/o) Al, some oxide film formation would be expected at the dispersoid surface and indeed is apparent from the significantly reduced current on the cathodic sweep compared to that in the anodic sweep and the decreasing anodic current with each cycle of potential. Although significantly less active than the bulk dispersoid material, the more active response of FVS0812, compared to pure Al and the matrix, reflects the presence of the more active dispersoid phase in the alloy. A similar influence of the dispersoids on the electrochemical behavior of the alloy was observed in acidic medium.[8] It is interesting that when the CV response of FVS0812 in this neutral medium is overlaid with a theoretical CV based on 73% of the bulk matrix CV response and 27% of the bulk dispersoid CV response, a very good fit is observed, as shown in Fig. 3. The similarity of these experimental and theoretical CVs for FVS0812 indicate that, by and large, the two phases within the alloy, rather than behaving synergistically, are not affecting each other in any notable way.

In summary, potentiodynamic studies support the sequence of activity obtained from the work at constant voltage, with the dispersoid displaying electrochemical activity significantly greater than alloy FVS0812, which is slightly greater than the almost equivalent activity of pure Al and the matrix material. The matrix material behaves very similarly to pure Al, forming a barrier oxide film in this medium. Evidence for some barrier oxide film formation at both the FVS0812 alloy and its dispersoid phase is clearly seen. The signatures of both the matrix and the dispersoid phases are seen in the CV response of alloy FVS0812.

Surface analysis.—Micrographs of cross sections of the oxide films formed in room temperature neutral boric acid/sodium borate at pure Al, the matrix, and FVS0812 are shown in Fig. 4 to 6. TEM analysis could not be performed on the bulk dispersoid material either before or after anodization as the extreme brittleness of this substrate prohibited the ultramicrotomed sectioning of the thin slices necessary for TEM work. Therefore, the thickness and nature of its oxide film are not known with certainty.

TEM micrographs of cross sections of the oxide films formed in neutral solution at 10 V at the matrix material and FVS0812, Fig. 4a and b, respectively, indicate relatively featureless films of uniform thicknesses of *ca.* 20 nm. These films appear to be very similar in thickness and in uniformity, to those grown on Al in several different barrier-film-forming solutions.[15,33-35] Importantly, no visible penetration of flaws to the substrates underlying the oxide films can be resolved at the 10 V anodizing potential. Also, no clear evidence for unreacted dispersoid, or of voids which might originally have contained the dispersoid, can be seen in the oxide film formed at the alloy at 10 V (Fig. 4b). This suggests that, while some of the Fe and V may have dissolved from the dispersoid, its principle mode of oxidation is to form an oxide film (consistent with the *i/t* and CV profiles in Fig. 1 and 2) which is indistinguishable by TEM analysis from the film formed at the

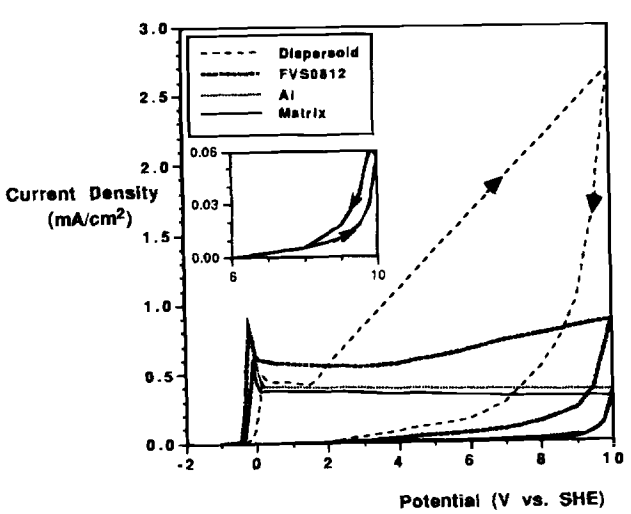

Fig. 2. Cyclic voltammograms of pure Al, the matrix, alloy FVS0812, and the dispersoid at 100 mV/s in 20°C neutral boric acid/sodium borate. Inset shows second cycle hysteresis behavior for matrix, using same axis units.

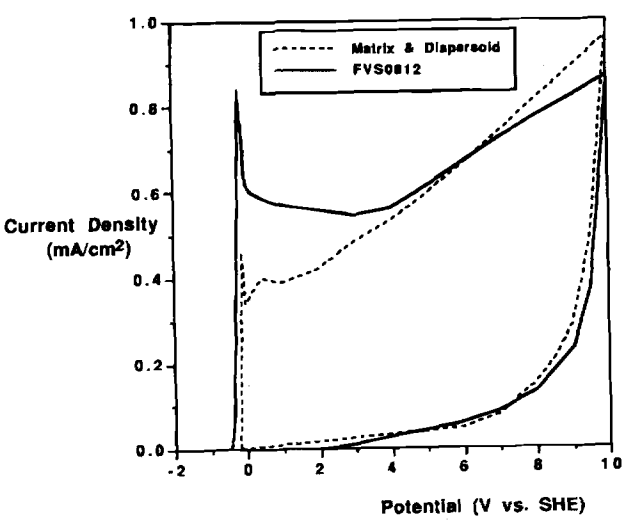

Fig. 3. Comparison of experimental CV of FVS0812 to theoretical CV of FVS0812 obtained by a mathematical combination of 73% of the CV response of the bulk matrix material and 27% of the CV response of the bulk dispersoid material.

matrix phase. However, it can be presumed that the loss of some Fe and V from the dispersoid during anodization of the alloy would lead to a flawed, lower density oxide film at the dispersoid sites, consistent with the higher rates of oxygen evolution observed at both the bulk dispersoid material and at the FVS0812 alloy.

The micrographs of the oxide formed to 50 V at pure Al and the matrix, Fig. 5a and b, respectively, show featureless, compact films of relatively uniform thickness which follow the profile of the substrate. EDX analysis of the films indicated only the presence of Al, and Cu from the supporting Au grid. The thicknesses of the oxide films formed at pure Al and the matrix appear to be quite similar, *i.e.*, *ca.* 85 to 90 nm for pure Al and 90 to 95 nm for the matrix. This similarity confirms the almost identical electrochemistry of pure Al and the matrix material, seen in both potentiodynamic and constant voltage experiments. The average thickness of 87 nm for pure Al yields an anodizing ratio (a_r) of 1.6 nm/V in this medium. This a_r value is greater than those often quoted in the literature, ranging from 1.2[33,35-37] to 1.4 nm/V,[33] for oxide films formed at pure Al by the application of a constant current until the desired potential is reached, followed by immediate removal of the electrode from the solution. The a_r obtained in the present work agrees more closely with an a_r of 1.6 to 1.7 nm/V reported for films formed at constant current to 50 V and then held at that potential for 1 to 2 h before removal from solution.[15] A thorough search of the literature has revealed that reported values of a_r for barrier oxide film formation depend upon the formation conditions employed. While this has been mentioned sporadically in early published work,[38] it does not appear to have been generally recognized in much of the more recent literature.

The oxide film formed at 50 V at FVS0812 is seen to be generally quite featureless (Fig. 5c), having a very similar

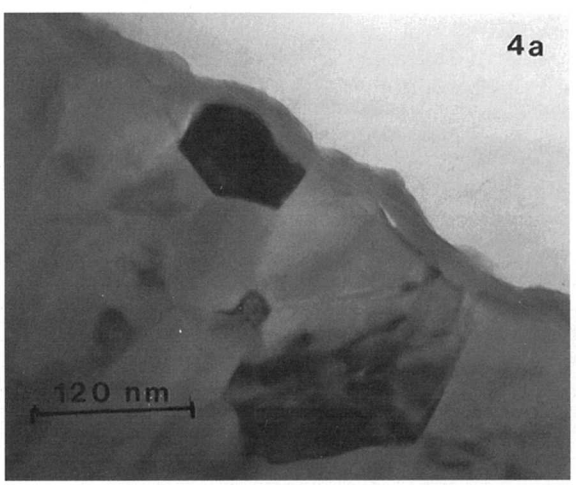

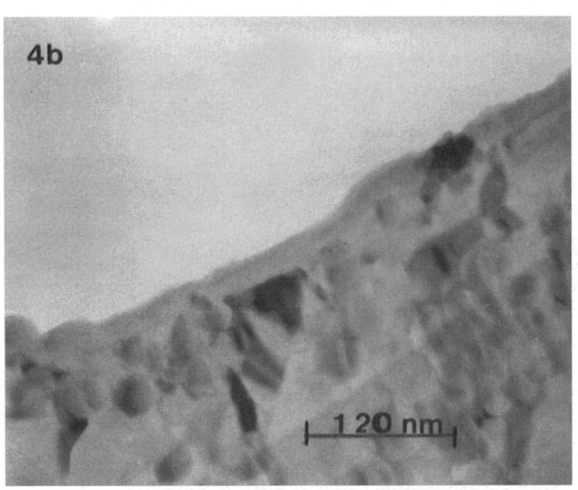

Fig. 4. Oxide film formed in 20°C neutral boric acid/sodium borate at 10 V: (a) at matrix for 1 h and (b) at FVS0812 for 2 h.

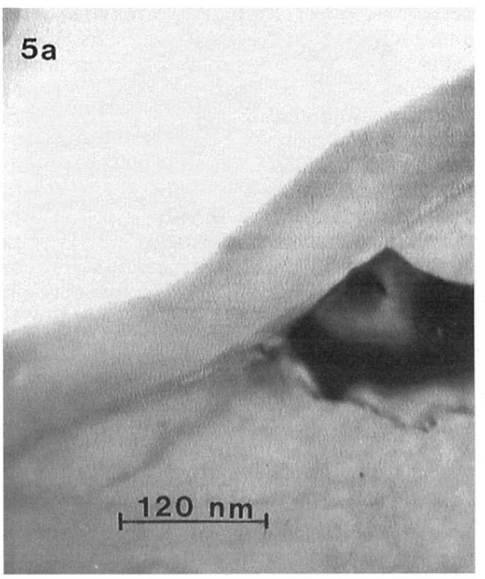

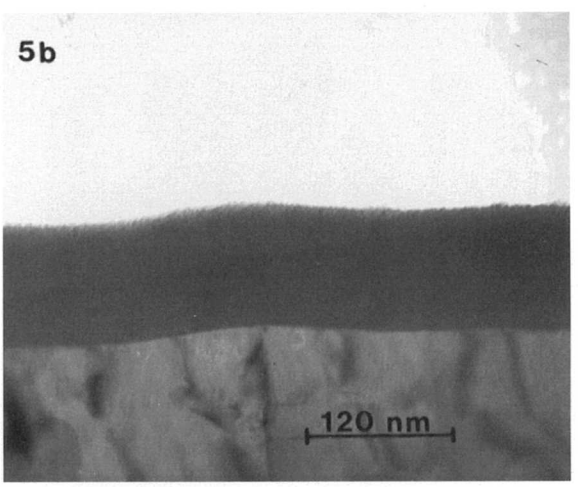

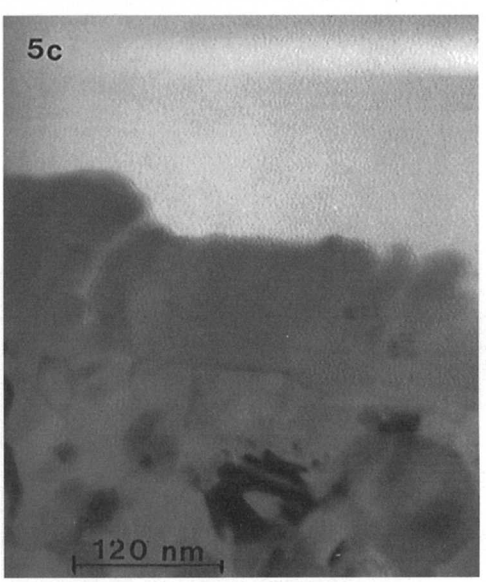

Fig. 5. Oxide film formed in 20°C neutral boric acid/sodium borate at 50 V for 2 h: (a) at pure Al, (b) at matrix, and (c) at FVS0812.

thickness to that formed at pure Al (Fig. 5a) and at the matrix material (Fig. 5b), *ca.* 93 nm. However, in some locations, some significant differences in the FVS0812 oxide film can now be seen (Fig. 6a and b). For example, Fig. 6a shows that occasional segments of the oxide film are thicker, up to 240 nm, and flaws which penetrate to the substrate can be observed in these regions of the film. Additionally, small, random segments of the oxide film are missing (Fig. 6a); these voids, such as shown in the right-hand side of Fig. 6a, have a very similar size to that of an individual dispersoid. This may suggest that these voids were originally filled by incompletely oxidized dispersoids, which were then lost from the film, either during the oxidation process, or during the preparation of the specimen for the microscopy work. In only infrequent locations, an individual dispersoid is observed to be still retained in the oxide film (Fig. 6b). This incorporation was confirmed by EDX analysis, which indicated the presence of Fe and V in addition to Al in the region of the oxide film in which the darker area, assumed to be the dispersoid material, was observed. EDX analysis of the featureless regions of the oxide film, comprising the majority of the film material, indicated only the presence of Al and Cu, again from the Cu grid.

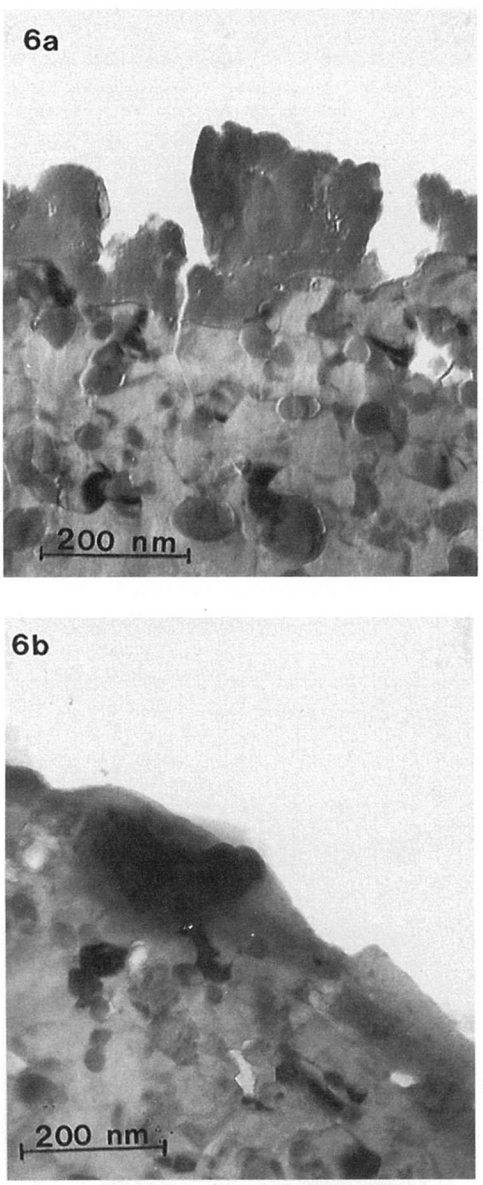

Fig. 6. Oxide film formed at FVS0812 in 20°C neutral borate solution at 50 V for 2 h: (a) featuring nonuniform film thickness and (b) featuring incorporated dispersoid.

A possible reason for the heterogeneous nature of the 50 V FVS0812 oxide film in some locations may be that during the more aggressive oxidation of the material at 50 V (*vs.* at 10 V), oxygen evolution at some dispersoid sites causes a significant increase in the local acidity. This could result in enough dissolution of the dispersoid to permit the dispersoid to fall out of the oxide film during either the anodization or the sectioning of the specimen, leaving the voids shown in Fig. 6a. Additionally, the local acidity near a dispersoid site would contribute to oxide dissolution and hence further oxide growth, similar to the processes occurring during porous film growth in acidic medium, resulting in the thicker regions of oxide displayed in Fig. 6a. At some other sites, retained dispersoids lead to the formation of a relatively thin oxide film at the dispersoid surface (Fig. 6b). In cases where the local acidity did not increase at a dispersoid site, the matrix surrounding the dispersoid, and the dispersoid itself, form the more uniform oxide film seen in Fig. 5c.

Overall, the surface analysis work confirmed the ability of both the matrix material and alloy FVS0812 to form a compact oxide film in borate solution, composed primarily of Al and O, similar to that formed at pure Al. In the present work, the average value of a_r, based on TEM measurements, is *ca.* 1.6 nm/V for pure Al, in agreement with the value reported in the literature for barrier oxide films formed on pure Al under similar conditions. Although virtually indistinguishable from oxide films formed to 10 V at pure Al and the matrix, the oxide film at FVS0812 differs significantly from films formed to 50 V at those two substrates. At 50 V, the oxide film at the alloy is no longer a fully intact barrier oxide film, as seen by the presence, in some locations, of flaws which penetrate to the substrate. Although the majority of the alloy's film is uniform in thickness, thicker regions of oxide are formed at infrequent intervals at the FVS0812 surface. The incomplete oxidation of dispersoids and their subsequent physical loss or retention in the oxide film formed at FVS0812 at 50 V is also suggested by the TEM study.

Electrochemical impedance spectroscopy.—EIS was used to probe further the differences between the surface oxides formed at the various substrates. In a series of experiments, anodic oxide films were grown by stepping the potential of the WE from open circuit to various upper potential limits. After 2 h at the upper limit, the potential of the WE was reduced to 0.1 V and impedance measurements were conducted at this value, a potential at which the neutral boric acid/sodium borate is nonaggressive to the substrates. Figure 7a and b shows the Bode plots illustrating the dependence of total impedance and phase angle, respectively, on the ac frequency for oxide films formed to a potential of 10 V at pure Al, the bulk matrix material, alloy FVS0812, and the bulk dispersoid material. Figure 8a and b represents, comparable plots for oxide films formed to a potential of 50 V. The -1 slopes of the impedance Bode plots, reflected in the values of the n exponents (Table II and III) for pure Al, the matrix, and FVS0812, indicate that the barrier oxide films at these substrates are responding capacitatively[39] over the frequency range of 10^1 to 10^3 Hz for films formed at a potential of 10 V and 10^1 to 10^4 Hz for films formed at a potential of 50 V. In contrast, the Bode slopes for the dispersoid material over the same frequency ranges are -0.82 and -0.78 at 10 and 50 V, respectively. The maximum values of the phase angles shown in Fig. 7b and 8b approach $-90°$ for pure Al, the matrix, and alloy FVS0812; the lowest value is $-84°$ at 50 V for FVS0812. In contrast, the maximum value of the phase angle achieved by the dispersoid is $-74°$. Phase angle values close to $-90°$ provide another indication of films functioning primarily capacitatively within the frequency range monitored. The different nature of the oxide formed at the dispersoid surface is therefore further highlighted by these data. It should be noted that a thinner barrier oxide film, having a concomitant decreased R and increased C, would result in smaller maximum value

of the phase angle.[40] However, because of the largely unknown nature of the oxide formed at the dispersoid surface, the interpretation of this data as reflecting the formation of significantly thinner film at the dispersoid compared to those formed at the surfaces of the other substrates cannot be considered conclusive.

The equivalent circuit which best fits the data obtained for the pure Al, matrix, and FVS0812 alloy substrates is one with a single *RC* time constant, consisting of a parallel combination of the oxide *R* and *C*, in series with the solution resistance. In contrast, the equivalent circuit for the dispersoid material suggests the presence of two time constants, with a second parallel *R* and *C* combination in series with the first. The existence of only one time constant for the barrier oxide film at both the matrix material and alloy FVS0812 is in agreement with the literature for pure Al. In the case of the dispersoid, the second time constant may reflect the presence of pores and flaws in the oxide formed at the dispersoid.

Tables II and III provide values for the *R* and *C* components of the oxide films formed at the four substrates after anodization in neutral boric acid/sodium borate at 10 and 50 V, respectively. These *R* and *C* values are calculated from the constant phase elements (CPE) and associated *n* exponent of each of the films. Strictly speaking, a CPE is equivalent to *C* of a film only when $n = 1$. The conversion of the *CPE* of the film to *C* is accomplished by the following equation[39]

$$C = CPE \sin (n\ 90) \quad [1]$$

Although the lowest value of the *n* exponent which can be used in the above equation is somewhat arbitrary, $0.8 < n < 1$ has been suggested as an appropriate range.[39]

The relationship between *C* and the thickness (*d*) of a nonconducting dielectric film is given by Eq. 2, where ϵ is the dielectric constant of the oxide, ϵ_0 is the permittivity of free space, 8.854×10^{-14} F/cm, and *A* is the area of the electrode

$$C/A = \epsilon\epsilon_0/d \quad [2]$$

It is seen in both Tables II and III that pure Al and the matrix material yield very similar C_1 values, *ca.* 5.7×10^{-7} F/cm^2 at 10 V and *ca.* 1.4×10^{-7} F/cm^2 at 50 V. This suggests a similar composition, ϵ, and *d* of the barrier oxides formed at pure Al and the matrix material, which is to be expected as the matrix material is *ca.* 99.4 a/o Al. These results are consistent with those obtained by TEM (Fig. 5a and b).

The C_1 of the oxide film formed at the alloy at both 10 and 50 V is notably larger than those of pure Al and the matrix by *ca.* 1.5 to 2 times (Tables II and III), while the dispersoid C_1 value is another 2.5 to 10 times larger than

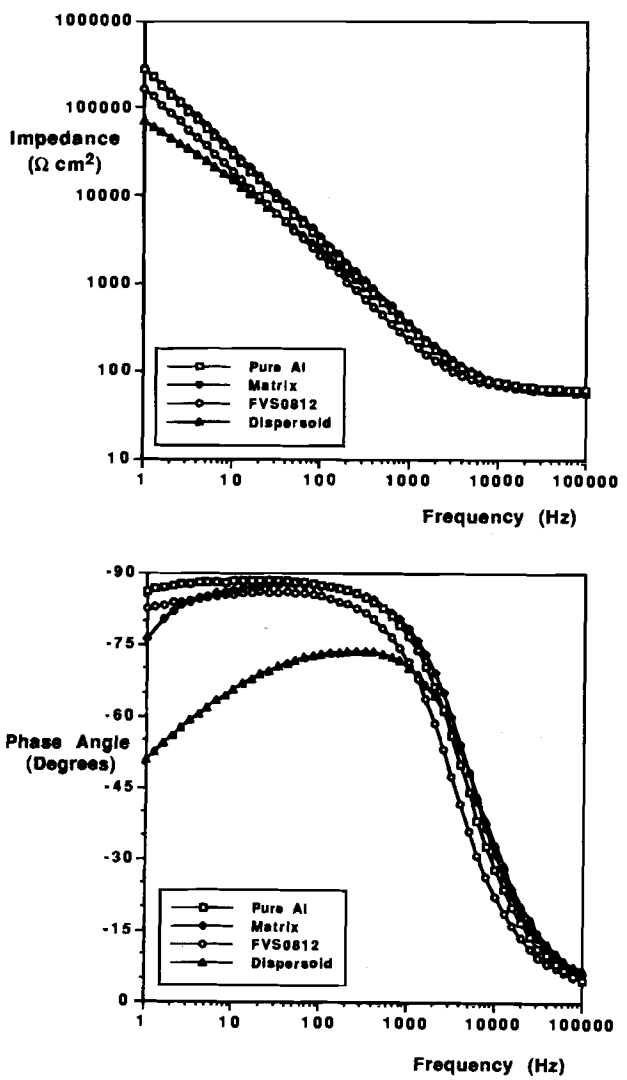

Fig. 7. Bode plots for oxide films formed at pure Al, the matrix, FVS0812, and the dispersoid at 10 V for 2 h in 20°C neutral boric acid/sodium borate. (a) Total impedance and (b) phase angle.

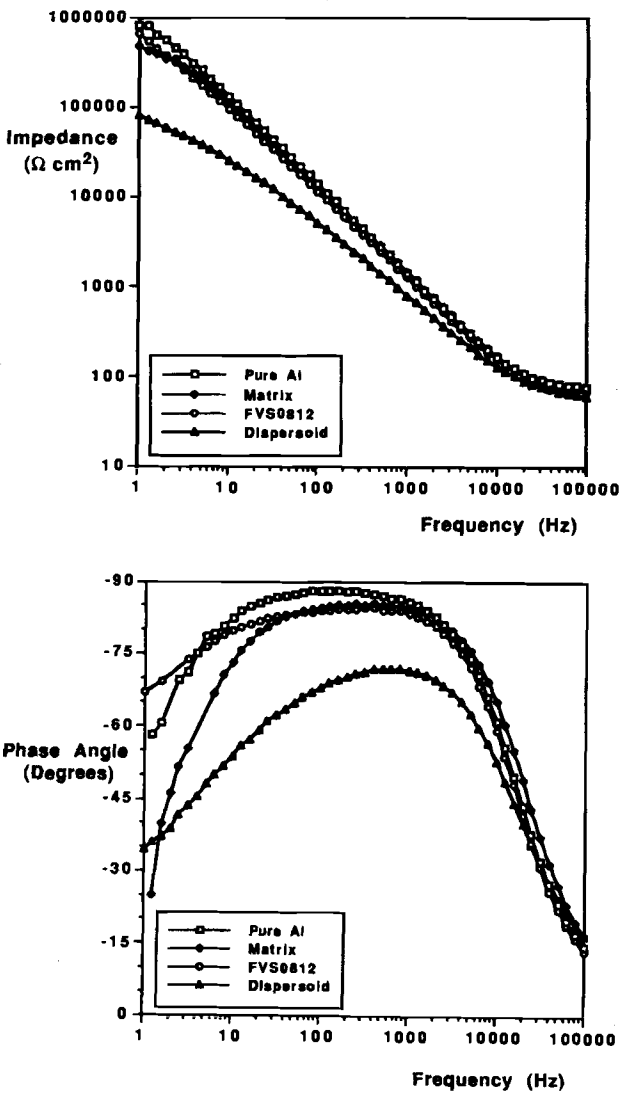

Fig. 8. Bode plots for oxide films formed at pure Al, the matrix, FVS0812 and the dispersoid at 50 V for 2 h in 20°C neutral boric acid/sodium borate: (a) total impedance and (b) phase angle.

Table II. Values of the components of equivalent circuits for oxide films formed at pure Al, the matrix, alloy FVS0812, and the dispersoid in neutral boric acid/sodium borate at 10 V for 2 h.

Substrate	R_1 (Ω cm^2)	C_1[a] (F cm^{-2})	n_1	R_2 (Ω cm^2)	C_2[a] (F cm^{-2})	n_2
Pure Al	7.3×10^6	5.9×10^{-7}	0.98			
Matrix	1.5×10^6	5.5×10^{-7}	0.98			
FVS0812	2.1×10^6	1.0×10^{-6}	0.96			
Dispersoid	1.5×10^5	2.4×10^{-6}	0.88	7.8×10^3	3.7×10^{-6}	0.86

[a] C is calculated from CPE and n using Eq. 1.

Table II. Values of components of equivalent circuits for oxide films formed at pure Al, the matrix, alloy FVS0812, and the dispersoid in neutral boric acid/sodium borate at 50 V for 2 h.

Substrate	R_1 (Ω cm^2)	C_1[a] (F cm^{-2})	n_1	R_2 (Ω cm^2)	C_2[a] (F cm^{-2})	n_2
Pure Al	1.3×10^6	1.3×10^{-7}	0.98			
Matrix	5.1×10^5	1.5×10^{-7}	0.96			
FVS0812	1.4×10^6	2.1×10^{-7}	0.94			
Dispersoid	1.0×10^5	2.1×10^{-6}	0.85	1.9×10^4	1.4×10^{-6}	0.83

[a] C is calculated from CPE and n using Eq. 1.

that of the alloy. This is another indication of the different nature of the oxide film formed at the dispersoid material compared to that at the other three substrates. The R_1 values, which are thought to reflect the resistance of the film as well as the reciprocal of the rate of any redox reactions which can occur at the potential used for impedance measurements, are quite similar for pure Al, the matrix material, and alloy FVS0812, but, again, are substantially different, *i.e.*, lower, for the dispersoid material. The higher C_1 and lower R_1 observed for the dispersoid may also reflect, in part, the higher surface area which may develop with time due to dissolution.

Interpretation of results.—Considering first the 10 V oxide films, the TEM analysis indicates that the thicknesses of the oxide films formed at the alloy and matrix material appear to be almost equivalent. However, the measured C of the 10 V oxide of alloy FVS0812 is greater by *ca.* 1.5 to 2 times than that of pure Al and the matrix material. The C of an oxide film will be dominated by the larger C of any regions of thinner oxide film.[40] The larger C of alloy FVS0812, compared to that of pure Al and the matrix, may therefore reflect the development of intermittent patches of thinner oxide film at the alloy surface (not seen by TEM), and/or by the penetration of the outer surface of the alloy's oxide by narrow flaws. This may occur particularly at the dispersoid sites, from which Fe and V may be partially dissolved, leaving a lower density oxide film at these locations.

Both explanations for the higher C of alloy FVS0812 would be consistent with the electrochemical behavior of FVS0812 in that, during anodization, a higher field would exist at the regions of thinner intact barrier oxide film, thus enhancing electronic conduction through the film and hence increasing the rate of oxygen evolution and other redox reactions at the surface. Such phenomena would be consistent with the higher leakage currents observed at constant voltage for FVS0812 compared to pure Al and the matrix (Fig. 1) and also with the increase of current with potential above *ca.* 3 V observable in the CV of FVS0812 (Fig. 2). In contrast, the uniform oxide thickness at the pure Al and matrix electrodes would result in a lower electric field across the oxide, compared to that at the thinner/flawed region of oxide at the alloy for the same applied potential, prohibiting significant oxygen evolution rates and resulting in lower leakage currents (Fig. 1) and a current plateau profile (Fig. 2), consistent with the observed electrochemical results.

In contrast to the alloy's oxide film formed at 10 V, the oxide film formed at 50 V contains some regions of obvious nonuniformity. Figure 6a features a segment of the FVS0812 oxide which contains regions more than twice as thick as the majority of the alloy's film thickness (Fig. 5c), as well as thinner regions of oxide, perhaps where incorporated dispersoids have been lost. A thin oxide region above a retained dispersoid in the 50 V film is suggested in Fig. 6b. Again, the C of the entire oxide film will reflect the C of those areas of visibly thinner, or flawed, oxide. Flaw penetration of the oxide at FVS0812 (Fig. 5c and 6a), but not at pure Al and the matrix (Fig. 5a and b), is clearly seen by TEM analysis. Oxide growth would be expected to be less uniform at the alloy, which contains 27 volume percent of spherical dispersoids, than at Al (99.999% pure) and the matrix material (99.4 a/o Al), where the absence of any significant impurities should promote uniform, relatively flawless oxide growth.

The reasons for the occasional nonuniform thickness, presence of flaws, and cracks in the alloy's oxide film when formed at 50 V, compared to the visibly unflawed nature and uniform thickness of the FVS0812 oxide formed at 10 V, are not completely understood. The explanation presented earlier that the high rate of oxygen evolution which can be sustained at the FVS0812 surface at 50 V may lead to isolated areas of high local acidity, hence promoting dissolution of the oxide and the onset of some porous film formation, may apply. Also, enhanced dissolution rates of the dispersoid may be expected at 50 V, especially at acidic pH.[8]

In summary, the increased C which is observed for the oxide formed at FVS0812, compared to that of pure Al and the matrix, is most probably due to the presence of the dispersoid phase within the alloy. Some dissolution of Fe and V, the loss of not fully oxidized individual dispersoids from the oxide film, or dispersoid retention, with the formation of thinner regions of oxide film, may all occur. Flaws at the surface of the alloy oxide, not seen by TEM analysis in a 10 V film, but visibly present in a 50 V film, could also contribute to the increased C of the alloy's oxide compared to that for oxide films formed at pure Al and the matrix. Compared to films formed at pure Al and the matrix material, an overall thinner and/or flawed oxide film at the alloy substrate surface would be consistent with the more active voltammogram for FVS0812 in Fig. 1, the higher leakage current in Fig. 2, and the larger values of C summarized in Tables II and III. The difficulty in forming a uniform, intact oxide film at the two-phase FVS0812 surface at 50 V in neutral borate solution can be considered as foretelling the difficulties in forming a thick, porous film at the alloy surface in more aggressive acidic media,[8] as is known to be the case in practice.

Conclusions

This work has focused on establishing the differences in barrier oxide films formed at FVS0812, a rapidly solidified, two-phase (matrix and dispersoid) Al-based alloy, at bulk forms of the alloy's matrix and dispersoid phases, and at pure Al. Electrochemical studies of these four substrates in 20°C neutral borate solutions have indicated a range of activities and degrees of passivating character of the oxide films. Oxide growth at constant voltage and potentiodynamic studies have shown the dispersoid material always to be the most active, followed by alloy FVS0812, while the matrix material and pure Al display the least, almost equivalent, activity. The more active electrochemical response of the dispersoid is considered to be due to a combination of substrate dissolution and high rates of oxygen evolution. The electrochemical response of alloy FVS0812 reflects the combination of the activities of both the matrix and dispersoid phases. Transmission electron micrographs of barrier oxide films formed at 10 V at the matrix material and FVS0812 in neutral borate solution show that the thicknesses of these uniform films are almost equivalent. Oxide films formed at 50 V at the FVS0812 substrate show some incorporation of dispersoids into the film, as well as occasional penetration of the outer film surface by flaws and infrequent regions of both thinner and thicker oxide. The increased capacitance of the FVS0812 oxide formed at 50 V, compared to that of pure Al and the matrix material, can be explained by both thinner oxide film at retained dispersoid sites and thinner oxide at regions from which dispersoids have been lost, as well as by the penetration of the surface oxide by flaws. This flawed oxide, nonuniform in thickness, suggests that the difficulties encountered in forming a thick, adherent, porous oxide film at FVS0812 in acidic media may be related to the difficulties experienced here in forming an intact, uniform barrier oxide at the alloy surface.

Acknowledgments

Acknowledgement is made to Allied Signal Incorporated for providing the FVS0812 alloy, matrix, and dispersoid samples, Don Steele and David Tessier of Alcan International Limited, Kingston R&D Center, for assistance and instruction with ultramicrotomy and transmission electron microscopy, and Dr. Petr Vanysek of Northern Illinois University for helpful discussions regarding impedance experiments. Financial assistance to V.I.B. and S.C.T. from the Natural Sciences and Engineering Council of Canada, and to S.C.T. from the Alberta Heritage Scholarship Fund, the Canadian Federation of University Women, the Izaak Walton Killam Memorial Scholarship Fund, the University of Calgary Faculty of Graduate Studies, the University of Calgary Department of Chemistry, and A. S. M. International "Calgary Chapter," is also gratefully acknowledged.

Manuscript submitted June 18, 1996; revised manuscript received Oct. 30, 1996.

The University of Calgary assisted in meeting the publication costs of this article.

LIST OF SYMBOLS

a_r	anodizing ratio
A	area
C	capacitance
CPE	constant phase element
CV	cyclic voltammetry
d	thickness
ϵ	dielectic constant
ϵ_o	permittivity of free space
EDX	energy dispersive x-ray analysis
EIS	electrochemical impedance spectroscopy
i	current density
ICP-AES	inductivity coupled plasma-atomic emission spectroscopy
n	value of exponent (0 to 1), defining nonideality of capacitive response
rms	root mean square
R	resistance
RE	reference electrode
SHE	standard hydrogen electrode
TEM	transmission electron microscopy
WE	working electrode
Z	impedance

REFERENCES

1. S. K. Das and L. A. Davis, *Mater. Sci. Eng.*, **98**, 1 (1988).
2. S. K. Das, R. L. Bye, and P. S. Gilman, *ibid.*, **A134**, 1103 (1991).
3. D. J. Skinner, M. S. Zedalis, and J. Peltier, in *Light Weight Alloys for Aerospace Applications*, E. W. Lee, E. H. Chia, and N. J. Kim, Editors, The Minerals, Metals & Materials Society, Warrendale, PA (1989).
4. D. J. Skinner, R. L. Bye, D. Raybould, and A. M. Brown, *Scr. Metall.*, **20**, 867 (1986).
5. D. J. Skinner, R. L. Bye, D. Raybould, A. M. Brown, and M. S. Zedalis, in *Processing of Structural Metals by Rapid Solidification, Proceedings of a Seven Session Symposium, on Enhanced Properties in Structural Metals via Rapid Solidification*, p. 291, ASM, Metals Park, OH (1987).
6. D. J. Skinner in *Dispersion Strengthened Aluminum Alloys*, Y.-W. Kim and W. M. Griffith, Editors, p. 181, The Mineral, Metals and Materials Society, Warrendale, PA (1988).
7. P. Gilman, *Met. Mater.*, 504 (1990).
8. S. C. Thomas and V. I. Birss, *This Journal*, **144**(4) (1997).
9. M. Zedalis, D. Rayould, D. J. Skinner, and S. K. Das, in *Processing of Structural Metals by Rapid Solidification. Proceedings of a Seven Session Symposium on Enhanced Properties in Structural Metals via Rapid Solidification*, pp. 347-354, ASM International, Metals Park, OH (1987).
10. S. K. Das, *J. Powder Metall.*, **24**, 175 (1988).
11. V. I. Birss, Internal Report, Allied-Signal Inc., Morristown, NJ (1990).
12. D. J. Skinner, Personal communication, 1993.
13. J. W. Diggle, T. C. Downie, and C. W. Goulding, *Chem. Rev.*, **69**, 365 (1969).
14. A. Despic and V. Parkhutik, in *Modern Aspects of Electrochemistry*, Vol. 20, J. O'M. Bockris, R. E. White, and B. E. Conway, Editors, p. 401, Plenum Press, New York (1989).
15. H. Takahashi and M. Nagayama, *Electrochim. Acta*, **23**, 279 (1978).
16. M. S. Hunter and P. Fowle, *This Journal*, **101**, 481 (1954).
17. G. E. Thompson and G. C. Wood, in *Treatise on Materials Science and Technology*, Vol. 23, J. C. Scully, Editor, Academic Press, Inc., New York (1983).
18. M. J. Dignam and D. Goad, *This Journal*, **113**, 381 (1966).
19. M. J. Dignam, *ibid.*, **109**, 184 (1962).
20. C. G. Dunn, *ibid.*, **115**, 219 (1968).
21. S. Sato, Y. Itoi, A. Hasumi, and E. Sato, *Electrochim. Acta*, **26**, 1303 (1981).
22. P. Ll. Cabot, J. A. Garrido, E. Perez, and J. Virgili, *Corros. Sci.*, **26**, 357 (1986).
23. P. Ll. Cabot, F. A. Centellas, J. A. Garrido, and E. Pérez, *J. Appl. Electrochem.*, **17**, 104 (1987).
24. Y. C. Cheng, H. C. Lin, and Y. H. Lee, *Tatung J.*, **18**, 141 (1988).
25. G. R. T. Schueller, S. R. Taylor, and E. Hajcsar, *This Journal*, **139**, 2799 (1992).
26. S. Piazza, A. Splendore, A. DiPaola, C. Sunseri, and F. DiQuarto, *ibid.*, **140**, 3146 (1993).
27. S. C. Thomas and V. I. Birss, in *Corrosion, Electrochemistry, and Catalysis of Metastable Metals and Intermetallics*, C. R. Clayton and K. Hashimoto, Editors, PV 93-30, p. 83, The Electrochemical Society Proceedings Series, Pennington, NJ (1993).
28. S. C. Thomas, V. I. Birss, D. Steele, and D. Tessier, *Microsc. Res. Tech.*, **31**, 285 (1995).
29. V. I. Birss, S. C. Thomas, and A. J. Zhang, *Electrochim. Acta*, **40**, 1551 (1995).
30. J. Bessone, C. Mayer, K. Juttner, and W. J. Lorenz, *ibid.*, **28**, 171 (1983).
31. M. M. Lohrengel, *Mater. Sci. Eng.*, **R11**, 243 (1993).
32. M. M. Lohrengel, *Electrochim. Acta*, **39**, 1265 (1994).
33. P. Skeldon, K. Shimizu, G. E. Thompson, and G. C. Wood, *Surf. Interface Anal.*, **5**, 252 (1983).
34. Y. Xu, G. E. Thompson, G. C. Wood, and B. Bethune, *Corros. Sci.*, **27**, 83 (1987).

35. K. Shimizu, K. Kobayashi, G. E. Thompson, and G. C. Wood, *Philos. Mag. B*, **64**, 345 (1991).
36. H. Habazaki, P. Skeldon, G. E. Thompson, G. C Wood, and K. Shimizu, *ibid.*, **71**, 81 (1995).
37. G. E. Thompson, P. Skeldon, K. Shimizu, and G. C. Wood, *Phil. Trans. R. Soc. London, Ser. A*, **350**, 143 (1995).
38. W. J. Bernard and J. W. Cook, *This Journal*, **106**, 643 (1959).
39. P. Vanysek, Unpublished work, Department of Chemistry, The University of Calgary, 1994.
40. P. Vanysek, Personal communication, 1994.

Electrochemical Behavior of Sol-Gel Produced Ni and Ni-Co Oxide Films

I. Serebrennikova* and V. I. Birss**

Department of Chemistry, University of Calgary, Calgary, Alberta, Canada T2N 1N4

ABSTRACT

Ni and mixed Ni-Co oxide films were formed at Pt substrates by the sol-gel technique and studied electrochemically in 1 *M* NaOH solutions. All sol-gel films under study have to be found amorphous. The charge densities of these films are quite high compared to oxides formed by the anodic oxidation of metallic substrates. Mixed Ni-Co oxide films display higher charge densities, broader CV peaks, and negatively shifted equilibrium potentials *vs.* pure Ni oxide films. At slow sweep rates, all films studied showed kinetically reversible surface electrochemical behavior. At higher sweep rates, the redox reactions became kinetically irreversible, being either surface reactions with no diffusion limitations or controlled by the diffusion rate of species inside the film. The effect of the oxide film formation conditions, *i.e.*, the withdrawal rate of the substrate from the sol solution and the firing temperature, on the electrochemical efficiency of the oxide films was also studied.

Introduction

Nickel oxide/hydroxide and mixed Ni-Co oxide films have been extensively studied in the past, primarily due to their numerous promising applications. These include their use as battery electrodes,[1] both in aqueous and nonaqueous media, with much work having been focused on the addition of Co to Ni oxides in order to improve their performance. The electrochromic oxidation/reduction in both cobalt and nickel oxide/hydroxide films, which occurs with the injection and expulsion of mobile ions,[2] has facilitated their applications in "smart windows,"[3] display panels,[4] and rearview mirrors.[4] Ni-Co-based alloys also appear to be very promising materials for water electrolysis because of their good electrocatalytic properties and reported stability for the oxygen[5-8] and hydrogen[9-11] evolution reactions. Cobalt based films are also widely used in recording media.[12]

The most important electrochemical process for Ni oxide electrodes, which occurs in alkaline solutions, can be described as [2]

$$Ni^{II}(OH)_2 + OH^- \rightleftarrows Ni^{III}OOH + H_2O + e^- \quad [1]$$

A similar reaction can be written for cobalt oxide electrodes[13]

$$3Co^{II}(OH)_2 + 2\,OH^- \rightleftarrows Co_3^{II,III}O_4 + 4H_2O + 2e^- \quad [2]$$

$$Co^{II}(OH)_2 + OH^- \rightleftarrows Co^{III}OOH + H_2O + e^- \quad [3]$$

and

$$Co^{III}OOH + OH^- \rightleftarrows Co^{IV}O_2 + H_2O + e^- \quad [4]$$

However, it is a well-established fact that these redox reactions are more complex than indicated here[1,14] and that they involve the intercalation/deintercalation of cations in basic solutions[15] in which the oxides are stable, *i.e.*, in simplified form[16]

$$Ni^{II}\text{ (or }Co^{III}\text{)oxide} + 1.5\,OH^- + 0.5Na^+ \rightleftarrows Ni^{III}\text{ (or }Co^{IV}\text{) oxide }(1.5\,OH^-)(0.5\,Na^+) + e^- \quad [5]$$

Nickel and cobalt oxide-hydroxide films can be prepared by the anodic oxidation of the metallic substrate,[1,5] cathodic precipitation,[1] electron-beam evaporation,[2,17] electrodeposition,[3,12] etc. Chemical deposition,[18] electrolytic deposition,[8,11] spray pyrolysis,[19,20] etc, are utilized to make mixed nickel-cobalt oxide films, which can also be formed by the anodic oxidation of polycrystalline and amorphous Ni-Co alloys.[10]

Our interest in nickel-cobalt based materials has arisen from the unique and promising properties of oxide films formed electrochemically in our laboratory at amorphous melt-spun Ni-Co based alloys.[16,21,22] It was found that, even in the presence of fairly high Co contents, the cyclic voltammetric (CV) response appeared to be primarily that of Ni. However, the amount of oxide which could be formed at these alloys with potential cycling was very high compared to that at pure nickel, with the growth characteristics, electrochromic properties, and film stability being much more similar to that of hydrous oxide films formed electrochemically at Co metal.[23] We therefore developed an interest in studying the properties of similar amorphous oxide films, this time formed by the sol-gel technique.

The sol-gel (SG) method was initially introduced as an energy saving approach in the preparation of glasses and ceramics.[24] The innovative aspect of the method involves mixing all components in solution, thus achieving homogeneity on the molecular scale. The gelation process results in the formation of an oxide network containing substantial amounts of water and organic residues. These are eliminated by the use of suitable drying techniques, yielding amorphous materials with a high degree of porosity.[25] The gels can be shaped into fibers, powders, or can be easily coated on a substrate.[25] SG techniques have been utilized to form single-component oxide materials,[26] as well as oxide mixtures, having an overall composition tailored by varying the ratios of the precursors in solution.[27] SG methods are very convenient for the preparation of thin films of high surface area amorphous oxide materials.

While quite a number of coatings have been formed using SG routes,[26,28,29] to our knowledge, there have been few reports as yet regarding the electrochemical response of oxide films produced in this manner. El Baydi *et al.*[30] prepared high surface area powders of $LaNiO_3$ and $NiCo_2O_4$ via the SG route and, while the oxidation/reduction characteristics of these materials were not examined, their catalytic activity for the oxygen evolution reaction in alkaline media was investigated. Liu *et al.*[31] investigated sol-gel formed nickel oxide films for use in electrochemi-

* Electrochemical Society Student Member.
** Electrochemical Society Active Member.